CURRENT DENSITY IMPEDANCE IMAGING

ADRIAN NACHMAN, ALEXANDRU TAMASAN, AND ALEXANDER TIMONOV

Abstract. We survey recent mathematical progress in Conductivity Imaging that is based on minimal interior knowledge of the Current Density field.

1. Introduction

The classical Electrical Impedance Tomography (EIT) problem seeks to obtain quantitative information on the electrical conductivity σ of a body from multiple boundary measurements of voltages and corresponding currents. Its extensive study has led to major mathematical advances on uniqueness and reconstruction methods for Inverse Problems with boundary data. See the excellent reviews [8], [7], and [13]. However, by now it is well understood that the problem is exponentially ill-posed, yielding images of low resolution away from the boundary [11], [33].

A new class of Inverse Problems seeks to significantly improve both the quantitative accuracy and the resolution of traditional Inverse Boundary Value Problems by using data which can be determined in the interior of the object. These have been dubbed Hybrid Methods, as they usually involve the combination of two different kinds of physical measurements. See, for instance, [16], [34], [9], [3],[12],[2],[4],[5], [47], [22] and further references below.

In this brief review, we present recent progress on such an approach for electric conductivity imaging, based on internal measurement of current densities. Such measurements have been possible since the early 1990 due to the pioneering work [17], [43] at the University of Toronto. The idea was to use Magnetic Resonance Imaging (MRI) in a novel way, to determine the magnetic flux density $\mathbf{B}$ induced by an applied current. We give a short description of this Current Density Imaging (CDI) technique in the Appendix.

We wish to stress that the mathematical inversion methods we present below do not necessarily depend on MRI: our discovery that it is possible to obtain high resolution images of conductivity from knowledge of the magnitude $|\mathbf{J}|$ of just one current density field may lead to simpler physical methodologies to obtain such data (see for instance [27]).

Two subclasses of conductivity imaging methods have been developed based on [17], [43]: the ones discussed here which use interior knowledge of the current density vector field (CDII), and the ones which use the measurement of only one component of the magnetic field, known as Magnetic Resonance Electric Impedance Tomography

AMS Subject Classification: 35R30, 35J60, 31A25, 62P10.
First author partly supported by an NSERC Discovery Grant.
Second author partly supported by NSF Grant No. 0905799.

(MREIT) [39, 41, 24, 28, 46]. The main advantage of MREIT over CDII methods is that they do not require two rotations of the subject (currently needed to obtain the current density field, see also the Appendix). While performing well in numerical simulations and experiments (with the aid of various ad hoc procedures), it is not known that these methods have unique solutions, except in some restrictive cases [29], [30].

The first work proposing to use CDI to image electrical conductivity was [48]. In [15] a perturbation method recovered the conductivity in the linearized case. Using the fact that $\mathbf{J}$ is normal to equipotential lines, the method in [25] recovered two dimensional conductivities. In [20] Seo et al. reduced the conductivity imaging problem to the Neumann problem for the 1-Laplacian (this will be detailed in Section 2); their examples of non- uniqueness and non-existence for this degenerate elliptic problem show that knowledge of the applied current at the boundary together with the magnitude of current density field inside is insufficient data to determine the conductivity. Instead, Seo et al proposed the "J- substitution" algorithm based on knowledge of the magnitude of two current density fields $|\mathbf{J}_1|, |\mathbf{J}_2|$; see also [19]. This algorithm has been shown in [21] to be convergent and, consequently, the conductivity is uniquely determined by the knowledge of the magnitude of two currents in the interior and of the currents at the boundary. The idea of using two non-parallel currents goes back to [42, Sec. 2.6.3]. In [40] the problem is reduced to a first order system of PDEs and several numerical reconstructions based on solving this system are proposed. In [18] Nachman et al. found a simple explicit formula for $\nabla \ln(\sigma)$ at each point in a region where two transversal current density vectors have been measured. This yielded an effective Current Density Impedance Imaging (CDII) method. (This formula, together with the reconstruction results from phantom experiments had been submitted in a patent application in 2003.) This reconstruction formula has been discovered independently by Lee in [26]. In [14] reconstructions based on experimental data were carefully validated against bench measurements. We refer the reader to that paper for convincing evidence that, unlike in EIT, the resolution in CDII is maintained away from the boundary.

What if only the magnitude $|\mathbf{J}|$ of just one current is known? In the following sections we describe the results on this problem from [35],[36],[37] and [38]. The key fact is that equipotential surfaces minimize the surface area induced by the Riemannian metric conformal to the Euclidean one $g = |\mathbf{J}|^{2/(d-1)} I$, where d is the dimension of the space. This approach reduces the conductivity imaging problem to a variational problem associated to the 1-Laplacian in the Riemannian metric g obtained from the given data.

2. Minimal surfaces in a Riemannian metric determined by the data

Let $\Omega \subset \mathbb{R}^d$, $d \geq 2$, be an open domain with connected, Lipschitz boundary $\partial\Omega$. The (unknonwn) conductivity σ is assumed isotropic, and essentially bounded away from infinity and zero; we use the notation $\sigma \in L^\infty_+(\Omega)$ to denote such functions. Let $\mathbf{J} \in L^2(\Omega; \mathbb{R}^d)$ be the current density field, $u \in H^1(\Omega)$ be the induced electric

potential and $\mathbf{E} = -\nabla u \in L^2(\Omega;\mathbb{R}^d)$ be the induced electric field in Ω. Further regularity will be assumed as stated in the theorems below.

From Ohm's law ($\mathbf{J} = -\sigma\mathbf{E}$) we have that, whenever $|\mathbf{E}| \neq 0$,

$$\sigma = \frac{|\mathbf{J}|}{|\mathbf{E}|} = \frac{|\mathbf{J}|}{|\nabla u|}. \tag{1}$$

If one can find the voltage potential from the data, then the formula (1) recovers the conductivity σ.

In the absence of charge sources/sinks the conservation law $\nabla\cdot\mathbf{J} = 0$ together with (1) lead to the singular, quasilinear, degenerate elliptic equation

$$\nabla\cdot\left(\frac{|\mathbf{J}|}{|\nabla u|}\nabla u\right) = 0. \tag{2}$$

The equation (2) with the above derivation first appeared in [20]. Our starting point was to realize its geometric significance:

Theorem 2.1 ([35])**.** *If $u \in C^1(\Omega)$ is an electric potential induced by the current density $\mathbf{J}$, and $|\mathbf{J}| > 0$ in Ω, then the level sets $\Sigma_\lambda := \{x \in \Omega : u(x) = \lambda\}$ are surfaces of zero mean curvature in the metric $g = |\mathbf{J}|^{2/(d-1)}I$. In particular they are critical surfaces for the area functional*

$$\boldsymbol{A}(\Sigma) = \int_\Sigma |\mathbf{J}| dS, \tag{3}$$

where dS is the Euclidean surface measure.

It was shown in [37] that the equipotential surfaces are not just critical surfaces but in fact they are area minimizers. (Note that $\mathbf{A}(\Sigma)$ is the area of Σ induced by the metric $g = |\mathbf{J}|^{2/(d-1)}I$. Note also that the functional in (3) is not convex with respect to the surface Σ.) The result relies on the co-area formula [32] and the proof adapts ideas of Bombieri et al. in [6]. We describe (compact) perturbations of a level set of u by the level set of an arbitrary functions v with the same trace at the boundary.

Theorem 2.2 ([37])**.** *Let $u \in C^{2,\delta}(\Omega)$ be the electric potential inside a $C^{1,\delta}$-smooth conductive body, generated while maintaining the voltage $f \in C^{2,\delta}(\partial\Omega)$ at the boundary, $0 < \delta < 1$. Assume $|\mathbf{J}| > 0$ in $\overline{\Omega}$. Let $\lambda \in Range(f)$ be such that $(d-1)$-Hausdorff measure of the set $f^{-1}(\lambda) \cap \partial\Omega$ is zero (valid a.e. $\lambda \in Range(f)$).*

Then, for any $v \in C^2(\overline{\Omega})$ with $v|_{\partial\Omega} = f$ and $|\nabla v| \neq 0$, we have

$$\boldsymbol{A}(u^{-1}(\lambda)) \leq \boldsymbol{A}(v^{-1}(\lambda)), \tag{4}$$

where $\boldsymbol{A}$ is defined in (3)*.*

3. A minimizing property of the electric potential and admissible data

Due to the degeneracy of (2), where the gradient is unbounded, and to its singularity where the gradient vanishes, the notion of solution needs to be defined carefully. The following example from [44] shows that if one considers solutions in the viscosity

sense (see, e.g., [10]) then there is non-uniqueness in the Dirichlet problem for (2) with $|J| \equiv 1$.

Let $= \{x \in R^2 : \ (x_1)^2 + (x_2)^2 < 1\}$ be the unit disk. The Dirichlet problem

$$\begin{aligned} \nabla \cdot \left(|\nabla u(x)|^{-1} \nabla u(x) \right) = 0, \ x \in \mathbb{D}, \\ u(x) = (x_1)^2 - (x_2)^2, \ x \in \partial \mathbb{D}, \end{aligned} \tag{5}$$

has a family of viscosity solutions (indexed in $\lambda \in [-1, 1]$):

$$u^\lambda(x) = \begin{cases} 2(x_1)^2 - 1, & if \quad |x_1| \geq \sqrt{\frac{1+\lambda}{2}}, \ |x_2| \leq \sqrt{\frac{1-\lambda}{2}}, \\ \lambda, & if \quad |x_1| \leq \sqrt{\frac{1+\lambda}{2}}, \ |x_2| \leq \sqrt{\frac{1-\lambda}{2}}, \\ 1 - 2(x_2)^2, & if \quad |x_1| \leq \sqrt{\frac{1+\lambda}{2}}, \ |x_2| \geq \sqrt{\frac{1-\lambda}{2}}. \end{cases} \tag{6}$$

However, it is only the solution corresponding to $\lambda = 0$ that minimizes the functional $\int_\Omega |\nabla u(x)| dx$ over the space of maps with bounded variation $BV(\mathbb{D})$ and the given trace on $\partial \mathbb{D}$ in (5).

Rather then try to solve the Dirichlet problem for (2), we consider instead the functional defined for an arbitrary $v \in H^1(\Omega)$ by

$$F[v] := \int_\Omega |\mathbf{J}(x)||\nabla v(x)| dx. \tag{7}$$

Formally the Euler-Lagrange for (7) is the 1-Laplacian (2). It turns out that the variational approach is well suited to our inverse problem: If $u \in H^1(\Omega)$ is the voltage potential induced by a current density field $\mathbf{J}$ generated while maintaining a boundary voltage $f \in H^{1/2}(\partial\Omega)$, then u minimizes F among all the competitors $v \in H^1(\Omega)$ with trace f at the boundary [36, Proposition 1.2]. Indeed, if $\sigma \in L^\infty_+(\Omega)$ is the unknown conductivity (such that $\mathbf{J} = -\sigma \nabla u$), then

$$\begin{aligned} \mathcal{F}[v] &= \int_\Omega \sigma |\nabla u| \cdot |\nabla v| dx \geq \int_\Omega \sigma |\nabla u \cdot \nabla v| dx \\ &\geq \int_\Omega \sigma \nabla u \cdot \nabla v dx = \int_{\partial\Omega} \sigma \frac{\partial u}{\partial \nu} v ds = \langle \Lambda_\sigma f, f \rangle = \mathcal{F}[u]. \end{aligned} \tag{8}$$

The example (5) above shows that the minimization of the functional (7) for an arbitrary data $|\mathbf{J}|$ in Ω and f at the boundary may lead to solutions which do not represent a voltage potential (since their gradients vanish in open sets while $|\mathbf{J}| \equiv 1$ does not). This motivates the following definition on the data: A pair $(f, a) \in H^{1/2}(\partial\Omega) \times L^2(\Omega)$ is called *admissible* if there exists a positive map $\sigma \in L^\infty_+(\Omega)$ such that, if $u \in H^1(\Omega)$ is the weak solution of $\nabla \cdot \sigma \nabla u = 0, \ u|_{\partial\Omega} = f$, then

$$|\sigma \nabla u| = a; \tag{9}$$

σ is called a *generating conductivity* and u is the *corresponding potential* for the pair of data (f, a) .

The example (5) above shows that the smooth pair $((x_1)^2 - (x_2)^2, 1)$ is not admissible since u^0 (the solution for $\lambda = 0$ in (6)) is the unique minimizer over $BV(\Omega)$ with

prescribed boundary data [45] and, for any $\sigma \in L^\infty_+(\Omega)$, the equation (9) cannot hold in the square $[-\frac{1}{\sqrt{2}}, \frac{1}{\sqrt{2}}] \times [-\frac{1}{\sqrt{2}}, \frac{1}{\sqrt{2}}]$.

Thus, the mere existence of a minimizer $u \in H^1(\Omega)$ for the functional in (7) is not sufficient to conclude existence of a generating conductivity. However, if we also have $|\mathbf{J}|/|\nabla u| \in L^\infty_+(\Omega)$ then the data is admissible [36, Proposition 1.2].

The result below gives the unique determination of a (Hölder continuous) conductivity from admissible data by using the minimization problem for the functional in (7); $W^{1,1}_+(\Omega)$ denotes the space of maps in $L^1(\Omega)$ with gradient in $L^1(\Omega)$, and with a negligible set of singular points.

Theorem 3.1 ([36]). *Let $\Omega \subset \mathbb{R}^d$, $d \geq 2$, be a domain with connected, $C^{1,\alpha}$- boundary and let $(f, |\mathbf{J}|) \in C^{1,\alpha}(\partial\Omega) \times C^\alpha(\overline{\Omega})$ be an admissible pair generated by some unknown $C^\alpha(\overline{\Omega})$ -conductivity. Assume that $|\mathbf{J}| > 0$ a.e. in Ω. Then the minimization problem*

$$argmin \left\{ \mathcal{F}[u] : \ u \in W^{1,1}_+(\Omega) \bigcap C(\overline{\Omega}), \ u|_{\partial\Omega} = f \right\}, \tag{10}$$

has a unique solution u_0. Moreover, $\sigma_0 = |\mathbf{J}|/|\nabla u_0|$ is the unique conductivity in $C^\alpha(\overline{\Omega})$ for which $|J|$ is the magnitude of the current density while maintaining the voltage f at the boundary.

Based on the results in [1], for simply connected planar domains there is a simple sufficient condition to ensure a non-vanishing current density field: we say that a map on the connected boundary is *almost two-to-one* if the set of local maxima is either one point or one connected arc. In two dimensions, the above uniqueness result can thus be simplified to:

Corollary 3.2 ([36]). *Let $\Omega \subset R^2$ be a simple connected domain with $C^{1,\alpha}$- boundary, $(f, |\mathbf{J}|) \in C^{1,\alpha}(\partial\Omega) \times C^\alpha(\overline{\Omega})$ be an admissible pair with f almost two-to-one. Then there is a unique positive conductivity in $C^\alpha(\overline{\Omega})$ for which $|\mathbf{J}|$ is the magnitude of the current density corresponding to the voltage f on the boundary. Moreover, the corresponding potential u_0 is the unique solution to the minimization problem (10).*

4. Reconstruction methods

4.1. **Level set methods.** In two dimensions, the level sets are geodesics. For smooth data $(f, |\mathbf{J}|) \in C^{2,\delta}(\partial\Omega) \times C^{1,\delta}(\Omega)$, they solve the geodesic system

$$\begin{aligned} \ddot{x} &= -\dot{x}^2 \tfrac{|\mathbf{J}|_x}{|\mathbf{J}|}(x,y) - 2\dot{x}\dot{y}\tfrac{|\mathbf{J}|_y}{|\mathbf{J}|}(x,y) + \dot{y}^2 \tfrac{|\mathbf{J}|_x}{|\mathbf{J}|}(x,y), \\ \ddot{y} &= \dot{x}^2 \tfrac{|\mathbf{J}|_y}{|\mathbf{J}|}(x,y) - 2\dot{x}\dot{y}\tfrac{|\mathbf{J}|_x}{|\mathbf{J}|}(x,y) - \dot{y}^2 \tfrac{|\mathbf{J}|_y}{|\mathbf{J}|}(x,y), \end{aligned} \tag{11}$$

where the dot denotes differentiation with the parameter $\frac{d}{dt}$.

The Cauchy boundary value problems for (11) recovers the equipotential lines originating on an arc Γ of the boundary and, via (1), recovers the conductivity in the region $\tilde{\Omega}$ spanned by these equipotential lines. This is a stable method. The following result is an immediate extension of Theorem 3.1 in [35], where is stated for almost two-to-one boundary voltage and Γ a maximal arc of monotony.

Theorem 4.1. *Let $\Omega \subset \mathbb{R}^2$ be a simply connected, bounded domain with a piecewise C^1-smooth boundary and $\Gamma \subset \partial\Omega$. Given $f \in C^2(\Gamma)$, $g \in C^1(\Omega)$, and $|\mathbf{J}| \in C^1(\overline{\Omega}) \cap C^2(\Omega)$, there exists a uniquely defined subregion $\tilde{\Omega} \subset \Omega$ and a unique pair $(\sigma, u) \in C^2(\tilde{\Omega}) \times C^2(\tilde{\Omega})$ such that u is σ-harmonic and $\sigma|\nabla u| = |\mathbf{J}|$ in $\tilde{\Omega}$, and $u|_\Gamma = f$ and $\partial_\nu u|_\Gamma = g$. Moreover, if f is almost two-to-one and Γ is a maximal arc of monotony, then the above holds with $\tilde{\Omega}$=Ω.*

The reconstruction based on Theorem 4.1 needs both the Dirichlet and Neumann data along Γ but, in contrast to the results in [25], only uses the magnitude $|\mathbf{J}|$.

Numerical results based on simulated data are shown in Section 5; see Figures 1 through 4.

Another method is based on the Dirichlet boundary value problem associated with (11). This only requires the interior data to be measured, while a desired voltage potential is maintained at the boundary. It has yielded the following uniqueness results for problems with partial data, which are important in applications.

Theorem 4.2 ([37])**.** *Let $\Omega \subset \mathbb{R}^2$ be a simply connected domain with $C^{2,\delta}$-boundary, $0 < \delta < 1$. For $i = 1, 2$ let $\sigma_i \in C^{2,\delta}(\Omega)$, u_i be σ_i-harmonic with $u_i|_{\partial\Omega} \in C^{2,\delta}(\partial\Omega)$ almost two-to-one, and $|\mathbf{J}_i| = |\sigma_i \nabla u_i|$. For $\alpha < \beta$ let*

$$\Omega_{\alpha,\beta} := \{x \in \overline{\Omega} : \ \alpha < u_1(x) < \beta\} \text{ and } \Gamma := \Omega_{\alpha,\beta} \cap \partial\Omega. \tag{12}$$

(i) Assume $u_1|_\Gamma = u_2|_\Gamma$ and $|\mathbf{J}_1| = |\mathbf{J}_2|$ in Ω. Then

$$u_1 = u_2 \text{ in } \Omega_{\alpha,\beta} \text{ and}$$
$$\sigma_1 = \sigma_2 \text{ in } \Omega_{\alpha,\beta}.$$

(ii) Assume $u_1|_\Gamma = u_2|_\Gamma$ and $|\mathbf{J}_1| = |\mathbf{J}_2|$ in the interior of $\Omega_{\alpha,\beta}$. Then

$$\{x \in \overline{\Omega} : \ \alpha < u_2(x) < \beta\} = \Omega_{\alpha,\beta}, \tag{13}$$
$$u_1 = u_2 \text{ in } \Omega_{\alpha,\beta} \text{ and} \tag{14}$$
$$\sigma_1 = \sigma_2 \text{ in } \Omega_{\alpha,\beta}. \tag{15}$$

The above results are constructive. The inversion method is based on solving two point boundary value problems to find geodesics joining pairs of equipotential points at the boundary. While for general manifolds with boundary the system (11) may not be uniquely solvable, using admissibility, the fact that the required geodesics are equipotential curves and the maximum principle we obtain the following result.(Note that this does not state that the metric $g = |\mathbf{J}|^2 I$ is simple, since uniqueness is only shown for geodesics joining equipotential pairs of boundary points.)

Theorem 4.3 ([37])**.** *Let $\Omega \subset \mathbb{R}^2$ be a simply connected domain with $C^{2,\delta}$-boundary, $0 < \delta < 1$. Let $(f, |\mathbf{J}|) \in C^{2,\delta}(\partial\Omega) \times C^{1,\delta}(\Omega)$ be an admissible pair with f almost two-to-one and let $(x_0, y_0), (x_1, y_1) \in \partial\Omega$ be such that $f(x_0, y_0) = f(x_1, y_1)$. Then the system (11) subject to the boundary conditions*

$$(x(0), y(0)) = (x_0, y_0) \text{ and } (x(1), y(1)) = (x_1, y_1), \tag{16}$$

has a unique solution $\gamma : [0,1] \to \Omega$, $\gamma(t) = (x(t), y(t))$. *Moreover, the map* $u : \Omega \to \mathbb{R}$ *is constant along* γ*:*

$$(u \circ \gamma)(t) = \lambda, \ t \in [0,1]. \tag{17}$$

Since solutions of (11) and (16) depend only on the values of $|\mathbf{J}|$ near the curve, we obtain partial reconstruction of σ from incomplete interior data. Assume that $|\mathbf{J}|$ is only known in a subregion $\tilde{\Omega}$ that contains regions of the type

$$\Omega_{\alpha,\beta} := \{x \in \overline{\Omega} : \alpha < u(x) < \beta\}, \tag{18}$$

for some unknown values α's and β's. We stress here that this property of $\tilde{\Omega}$ need not be assumed a priori: the method determines from the data if $\tilde{\Omega}$ contains regions of the type (18), and, if so, recovers all the (maximal) intervals (α, β), their corresponding $\Omega_{\alpha,\beta}$ and the conductivity therein. If $\tilde{\Omega}$ does not contain regions of type (18), then the incomplete interior data is insufficient to recover the conductivity in any subregion.

The reconstruction procedure starts by extending $|\mathbf{J}|$ to all of Ω. To find the equipotential curves which lie entirely in $\tilde{\Omega}$ one solves (11) subject to (16), for each pair of equipotential boundary points. If the solution lies in the interior of $\tilde{\Omega}$, then it is the correct level curve joining those two boundary points. If the calculated curve passes outside $\tilde{\Omega}$ (or touches its boundary) then it is dependent on the extension of $|\mathbf{J}|$ and we discard it. An interval (α, β) of voltages defines a set $\Omega_{\alpha,\beta}$ as in (18) provided that, for each $\lambda \in (\alpha, \beta)$, the calculated λ-equipotential curve lies entirely in the interior of $\tilde{\Omega}$. If $\tilde{\Omega}$ contains no entire equipotential curves, then all the calculated solutions will be discarded; see Figures 5 and 6.

4.2. **Variational approaches.** The reconstruction methods described in Section 4.1 recover u one level set at a time. The methods based on the minimization problem in Theorem 3.1 recover all the equipotential sets at once. We use a nonnegative weight $a \in L^2(\Omega)$ to denote $|\mathbf{J}|$ in the functional (7).

Two methods have been proposed. The one in [36] is based on the following minimization property.

Lemma 4.4. *Assume that* $v \in H^1(\Omega)$ *is such that* $\frac{a}{|\nabla v|} \in L^\infty_+(\Omega)$ *and let* $u \in H^1(\Omega)$ *be the weak solution of*

$$\begin{cases} \nabla \cdot \frac{a}{|\nabla v|} \nabla u = 0 \text{ in } \Omega, \\ u|_{\partial\Omega} = v|_{\partial\Omega}. \end{cases}$$

Then the following inequalities hold:

$$\int_\Omega a|\nabla u| dx \leq \int_\Omega a|\nabla v| dx; \tag{19}$$

$$\int_\Omega a|\nabla u| dx \geq \int_\Omega \frac{a}{|\nabla v|}|\nabla u|^2 dx; \tag{20}$$

$$\frac{1}{2}\int_\Omega \left(a|\nabla v| - \frac{a}{|\nabla v|}|\nabla u|^2\right) dx \qquad \leq \int_\Omega \left(a|\nabla v| - a|\nabla u|\right) dx$$

$$\leq \int_\Omega \left(a|\nabla v| - \tfrac{a}{|\nabla v|}|\nabla u|^2\right) dx. \tag{21}$$

We also have the identity:

$$\int_\Omega \left(a|\nabla v| - \frac{a}{|\nabla v|}|\nabla u|^2\right) dx = \int_\Omega \frac{a}{|\nabla v|}|\nabla v - \nabla u|^2 dx. \tag{22}$$

Moreover, equality in either of (19) or (20) holds if and only if $u = v$.

Algorithm 1: Let $(f, a) \in H^{1/2}(\partial\Omega) \times L^2(\Omega)$ be an admissible pair. For $u_{n-1} \in H^1(\Omega)$ given such that $\frac{a}{|\nabla u_{n-1}|} \in L^\infty_+(\Omega)$, define

$$\sigma_n = \frac{a}{|\nabla u_{n-1}|} \tag{23}$$

and construct u_n as the unique solution to

$$\begin{cases} \nabla \cdot \sigma_n \nabla u_n = 0, \\ u_n|_{\partial\Omega} = f. \end{cases}$$

Now iterate.

We need conditions to ensure that each iterate satisfies $\frac{a}{|\nabla u_n|} \in L^\infty_+(\Omega)$. In two dimensions, an almost two-to-one boundary voltage f is sufficient for this to hold, and further a posteriori sufficient conditions ensure convergence [36]. Figure 7 and 8 show reconstructions based on Algorithm 1.

The second variational approach is based on the minimization problem for the regularized functional defined for $\delta \geq 0$ and $\epsilon > 0$ as

$$\mathcal{F}^\delta_\epsilon[u; a] = \int_\Omega a \max\{|\nabla u|, \delta\} dx + \epsilon \int_\Omega |\nabla u|^2 dx. \tag{24}$$

For any $(f, a) \in H^{1/2}(\partial\Omega) \times L^2(\Omega)$ (not necessarily admissible) the problem

$$\min\left\{\mathcal{F}^\delta_\epsilon[u; a] : \, u \in H^1(\Omega), \, u|_{\partial\Omega} = f\right\} \tag{25}$$

has a unique solution [38, Proposition 5].

If the data is admissible and the interior data is essentially bounded away from zero, then the following stability result holds.

Theorem 4.5 ([38])**.** *Let $(f, a) \in H^{1/2}(\partial\Omega) \times L^2(\Omega)$ be admissible, and assume*

$$\mathit{essinf}(a) \geq \alpha, \tag{26}$$

for some $\alpha > 0$. Then there is a $\delta > 0$ such that the followings hold:

(i) For any $\{a_n\} \subset L^2(\Omega)$, a sequence with $a_n \to a$ in $L^2(\Omega)$, if we choose $\epsilon_n \downarrow 0$ in such a way that

$$\lim_{n\to\infty} \frac{\|a - a_n\|^2}{\epsilon_n} = 0,$$

and, for each n, let u_{ϵ_n} *be the solution of the minimization problem*

$$u_{\epsilon_n} = argmin\{\mathcal{F}^{\delta}_{\epsilon_n}[u; a_n] : \ u \in H^1(\Omega),\ u|_{\partial\Omega} = f\}.$$

Then

$$\begin{aligned}\liminf_{n\to\infty} \mathcal{F}^{\delta}_{\epsilon_n}[u_{\epsilon_n}; a_n] = \liminf_{n\to\infty} \mathcal{F}^{\delta}_{0}[u_{\epsilon_n}; a_n] &= \min\{\mathcal{F}^{\delta}_{0}[u; a] : \ u \in H^1(\Omega),\ u|_{\partial\Omega} = f\} \\ &= \min\{\mathcal{F}^{0}_{0}[u; a] : \ u \in H^1(\Omega),\ u|_{\partial\Omega} = f\}.\end{aligned}$$

(ii) There is a subsequence $\{u_{\epsilon_k}\}$ *convergent in* $L^q(\Omega)$ *to some* $u^* \in L^q(\Omega) \cap BV(\Omega)$, $1 \le q < d/(d-1)$.

(iii) If $u^* \in H^1(\Omega) \cap C(\overline{\Omega})$ *then* u^* *is the potential corresponding to the pair* (f, a).

5. Reconstruction from simulated data

5.1. **Equipotential lines methods.** We simulate a conductivity σ using a CT-image of a human torso. The density distribution in the original CT image has been scaled to a conductivity distribution ranging from 1 to 1.8 S/m, see Figure 1.

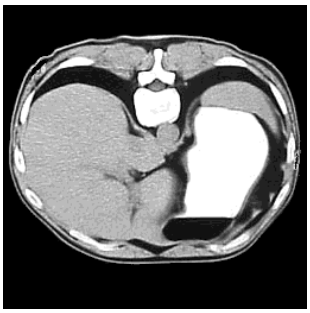

Figure 1. The original conductivity distribution to be reconstructed.

Partial Cauchy data: To implement to method based on Theorem 4.1, we consider two experiments. They use the same conductivity but the interior data $|\mathbf{J}|$ shown in Figure 2 is generated by solving two distinct Dirichlet problems. On the left the boundary voltage is almost two-to-one, while on the right it is not.

The equipotential lines (characteristics) are calculated by solving the initial value problem for (11) with Cauchy data on the left side of the rectangle. Figure 3 on the left shows the equipotential lines from the corresponding two experiments. Note that when $|\mathbf{J}|$ is generated by boundary data which does not satisfy the almost two-to-one condition, the equipotential lines originating on the left side of the rectangle do not fill the lower right corner of the rectangle.

Figure 4 shows reconstructed conductivities in the four experiments. The two pictures on the left are based on noiseless and noisy data, with an almost two-to-one boundary voltage. The two pictures on the right are based on noiseless and noisy data and a boundary voltage which is not almost two-to-one. The lower right hand corner show meaningless computational artifacts.

Dirichlet data: The reconstruction based on Theorem 4.3 solves a family of two point boundary value problems for the system (11). The interior data $|\mathbf{J}|$ generated by

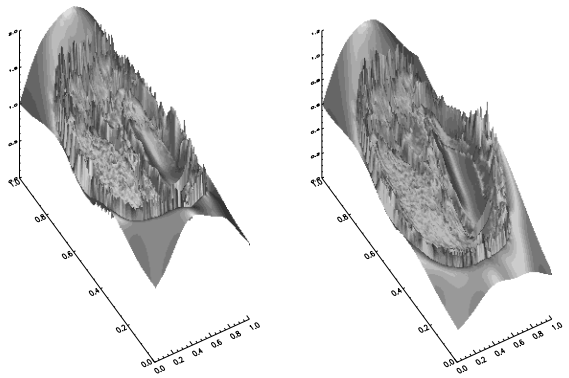

FIGURE 2. Interior data $|\mathbf{J}|$: On the left the boundary voltage is almost 2-1, while on the right it is not.

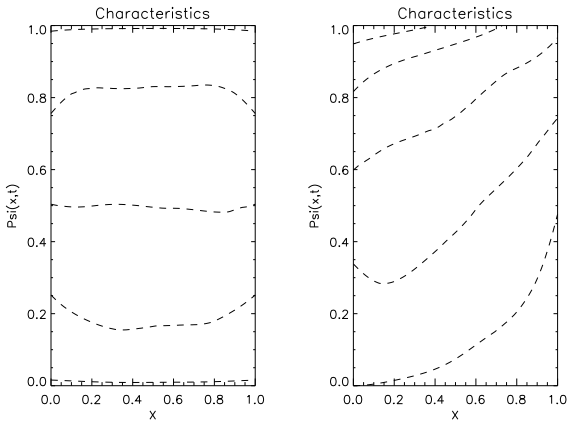

FIGURE 3. Interior data $|\mathbf{J}|$: On the left the boundary voltage is almost 2-1, while on the right it is not.

the almost two-to-one boundary data has been used (Left image in Figure 2). Figure 5 shows the calculated characteristics for full interior data and partial boundary data. Figure 6 shows the reconstructed conductivity from partial interior and boundary data.

5.2. **Variational Method.** Numerical reconstructions here are based on the Algorithm 1. Figure 7 shows the original conductivity (to be reconstructed) on the left, and various iterates in the Algorithm 1. Figure 8 shows a slice through the middle of the rectangle for the various iterates.

6. Appendix: Current Density Imaging

In this section we briefly describe the way the interior data is currently acquired using a Magnetic Resonance Imager [43].

FIGURE 4. Reconstructed conductivities. Left two pictures: noiseless (left) and noisy data; almost 2-1 case. Right two pictures: noiseless (left) and noisy data; non almost 2-1 case.

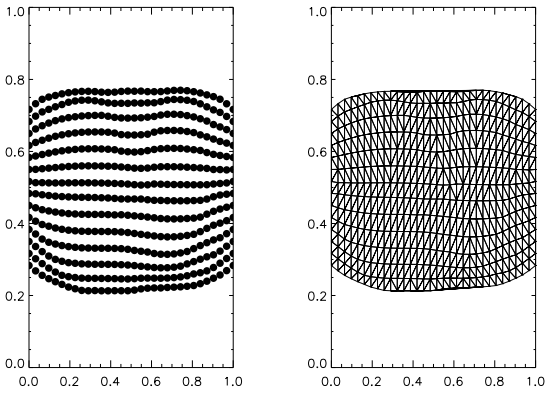

FIGURE 5. Equipotential lines calculated by solving two point boundary value problems(left) and the triangulated area spanned by these lines (right).

In the three dimensional space, orient the z-axis along the main static magnetic field of the MRI. Upon injecting a low frequency current I_+, the induced magnetic field $\mathbf{B} = (B_x, B_y, B_z)$ alters the resonance frequency of protons. Intuitively, the main static magnetic field is modified by the additional B_z. This produces a phase change in the rotating transverse component of the magnetic resonance signal M, represented as a complex number. More precisely, the phase change in the transversal plane $z = z_0$ is proportional with the component B_z and the duration T of the injected current:

$$M_+(x, y, z_0) = M(x, y, z_0)e^{i\gamma B_z(x,y,z_0)T+i\varphi_0};$$

here φ_0 is the phase due to the original magnetic field (in the absence of the applied current) and γ (the so-called gyromagnetic ratio) is known. By applying the inversely

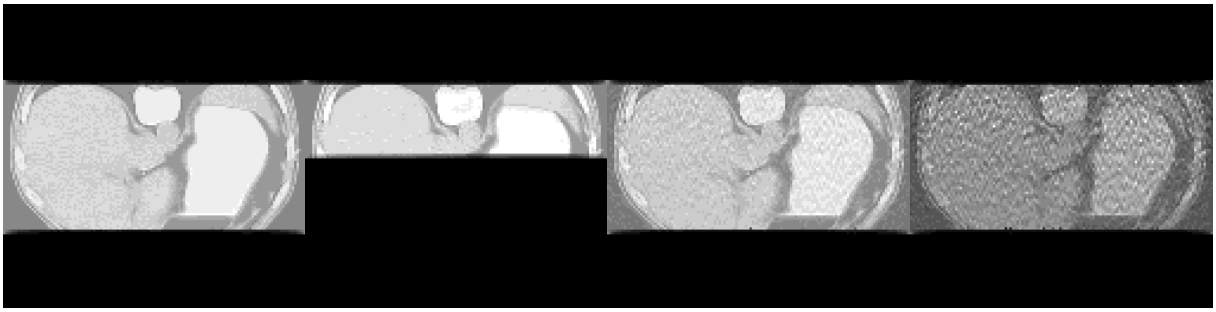

FIGURE 6. Reconstructed conductivity from partial interior and boundary data: noiseless (two pictures on the left) and noisy (two pictures on the right).

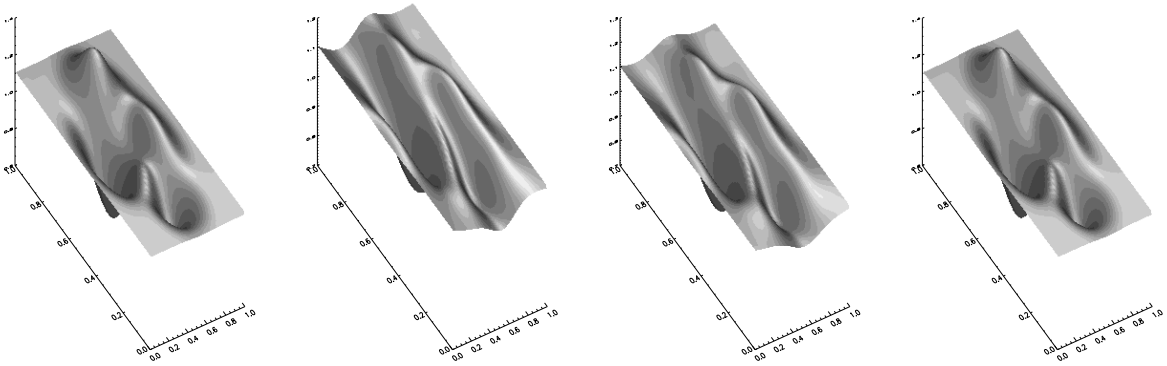

FIGURE 7. From the left: 1st image is the original conductivity , 2nd image is the first iterate, 3rd image is the fifth iterate and 4th image is the fiftieth iterate in Algorithm 1.

polarized current I_- for the same duration T, one obtains

$$M_-(x,y,z_0) = M(x,y,z_0)e^{-i\gamma B_z(x,y,z_0)T + i\varphi_0}.$$

Therefore, one can recover B_z from the MRI phase image as

$$B_z(x,y,z_0) = \frac{1}{2\gamma T}\mathbb{I}m \log\left(\frac{M_+(x,y,z_0)}{M_-(x,y,z_0)}\right),$$

where log denotes an analytic branch of the complex logarithm. In practice, one uses a "phase unwrapping" algorithm to determine a continuous branch.

With two rotations of the object one determines all the components of $\mathbf{B}$ and the current density field is then calculated based on Ampere's law, $\mathbf{J} = \frac{1}{\mu_0}\nabla \times \mathbf{B}$, where μ_0 is the magnetic constant.

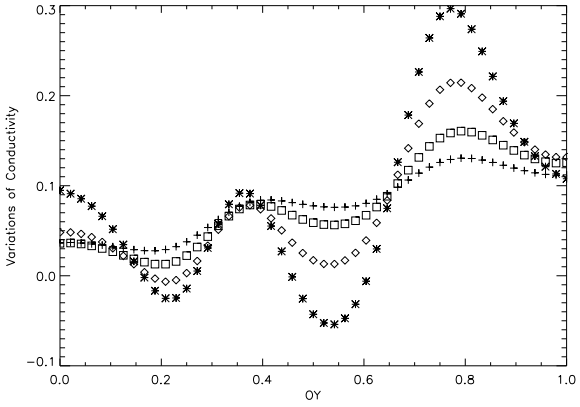

FIGURE 8. The vertical slices of variations of conductivity over the unit one reconstructed from the noiseless data: crosses - the initial approximation, squares - after 5 iterates, diamonds - after 50 iterates, and stars - after 100 iterates. The latter coincides with the simulated conductivity.

ACKNOWLEDGMENTS

Progress on some of these problems was accomplished during the BIRS workshop on "Inverse Problems: Recent Progress and New Challenges" (08w5065), November 16-21, 2008. Some of the results were presented at the BIRS workshop on "Mathematical Methods in Emerging Modalities of Medical Imaging" (09w5017), Banff, Alberta, Canada, Oct 25-30, 2009. The authors would like to thank the Banff International Research Station for the wonderful hospitality and excellent working environment.

REFERENCES

[1] G. ALESSANDRINI, *An identification problem for an elliptic equation in two variables*, Annali di matematica pura ed applicata, **145** (1986), pp. 265–295.

[2] H. AMMARI, Y. CAPDEBOSCQ, H. KANG, AND A. KOZHEMIAK, *Mathematical models and reconstruction methods in magneto-acouostic imaging*, European J. Appl. Math., **20**(2009), pp. 303–317.

[3] H. AMMARI, E. BONNETIER, Y. CAPDEBOSCQ, M. TANTER, AND M. FINK, *Electrical Impedance Tomography by Elastic Deformation*, SIAM J. Appl. Math., **68** (2008), pp.1557–1573.

[4] G. BAL AND J.C. SCHOTLAND, *Inverse Scattering and Acousto-Optic Imaging*, Phys. Rev. Letters **104**(2010), 043902.

[5] G. BAL AND G. UHLMANN, *Inverse Diffusion Theory of Photoacoustics*, Inverse Problems **26**(2010), 085010.

[6] E. BOMBIERI, E. DE GIORGI AND E. GIUSTI, *Minimal Cones and the Bernstein Problem*, Inventiones Math. **7** (1969), pp. 243–268.

[7] L. BORCEA, *Electrical impedance tomography*, Inverse Problems **18**(2002), R99–R136.

[8] M. CHENEY, D. ISAACSON, AND J. C. NEWELL, *Electrical Impedance Tomography*, SIAM Rev. **41**(1999), no.1, 85 –101.

[9] B. T. Cox, S. R. Arridge, K. P. Kostli, and P. C.Beard,*2D quantitative photoacoustic image reconstruction of absorption distributions in scattering media using a simple iterative method*, Applied Optics **45**(2006), 1866–1875.

[10] M. G. Crandall, H. Ishii, and P. -L. Lions *User's guide to viscosity solutions of second order partial differential equations*,Bull. Amer. Math. Soc. **27**(1992), 1–67.

[11] D. Isaacson and M. Cheney, *Effects of measurement precision and finite numbers of electrodes on linear impedance imaging algorithms,* SIAM J. Appl. Math. 51 (1991), no. 6, 1705–1731.

[12] B. Gebauer and O. Scherzer, *Impedance-acoustic tomography*, SIAM J. Appl. Math., **69** (2008), pp. 565–576.

[13] A. Greenleaf, Y. Kurylev, M. Lassas, and G. Uhlmann, *Invisibility and inverse problems*, Bull. Amer. Math. Soc. 46 (2009), 55-97.

[14] K. F. Hasanov, A. W. Ma, A. I. Nachman, and M. J. Joy, *Current Density Impedance Imaging*, IEEE Trans. Med. Imag. **27**(2008),pp. 1301–1309.

[15] Y.Z. Ider and Ö. Birgül , *Use of the magnetic field generated by the internal distribution of injected currents for Electrical Impedance Tomography(MR-EIT)*, Elektrik **6** (1998), 215–225

[16] L. Ji, J. R. McLaughlin, D. Renzi and J.-R. Yoon, *Interior elastodynamics inverse problems: shear wave speed reconstruction in transient elastography*, Inverse Problems **19**(2003), S1S29.

[17] M. L. Joy, G. C. Scott, and M. Henkelman, *In vivo detection of applied electric currents by magnetic resonance imaging*, Magnetic Resonance Imaging, **7** (1989), pp. 89–94.

[18] M. J. Joy, A. I. Nachman, K. F. Hasanov, R. S. Yoon, and A. W. Ma, *A new approach to Current Density Impedance Imaging (CDII)*, Proceedings ISMRM, No. 356, Kyoto, Japan, 2004.

[19] H.S. Khang, B.I. Lee, S. H. Oh, E.J. Woo, S. Y. Lee, M.H. Cho, O. I. Kwon, J.R. Yoon, and J.K. Seo, *J-substitution algorithm in magnetic resonance electrical impedance tomography (MREIT): Phantom experiments for static resistivity images*, IEEE Trans. Med. Imag., **21**(2002), no. 6, pp. 695 –702.

[20] S. Kim, O. Kwon, J. K. Seo, and J. R. Yoon, *On a nonlinear partial differential equation arising in magnetic resonance electrical impedance tomography*, SIAM J. Math. Anal., **34** (2002), pp. 511–526.

[21] Y.J. Kim, O. Kwon, J. K. Seo, and E. J. Woo, *Uniqueness and convergence of conductivity image reconstruction in magnetic resonance electrical impedance tomography*, Inverse Problems **19**(2003), no. 5, 1213-1225.

[22] P. Kuchment and L. Kunyansky, *2D and 3D reconstructions in acousto-electric tomography*, preprint.

[23] O. Kwon, E. J. Woo, J. R. Yoon, and J. K. Seo, *Magnetic resonance electric impedance tomography (MREIT): Simulation study of J-substitution algorithm*, IEEE Trans. Biomed. Eng., **49** (2002), pp. 160–167

[24] O. Kwon, C. J. Park, E.J. Park, J. K. Seo, and E. J. Woo , *Electrical conductivity imaging using a variational method in B_z-based MREIT*, Inverse Problems **21** (2005), pp. 969–980.

[25] O. Kwon, J. Y Lee, and J. R. Yoon, *Equipotential line method for magnetic resonance electrical impedance tomography*, Inverse Problems **18** (2002), pp. 1089-1100

[26] J. Y. Lee *A reconstruction formula and uniqueness of conductivity in MREIT using two internal current distributions*, Inverse Problems **20** (2004), pp. 847–858

[27] X. Li, Y. Xu and B. He, *Imaging Electrical Impedance from Acoustic Measurements by Means of Magnetoacoustic Tomography with Magnetic Induction (MAT-MI)*, IEEE Trans. Biomed. Eng. **54**(2007), pp. 323-330.

[28] J. J. Liu, H. C. Pyo, J. K. Seo, and E. J. Woo, *Convergence properties and stability issues in MREIT algorithm*, Contemporaty Mathematics **25** (2006), 168–176.

[29] J. J. Liu, J. K. Seo, M. Sini and E. J. Woo, *On the convergence of the harmonic Bz Algorithm in Magnetic Resonance Imaging*, SIAM J. Appl. Math. **67** (2007), 1259–1282.
[30] J. J. Liu, J. K. Seo, and E. J. Woo, *A Posteriori Error Estimate and Convergence Analysis for Conductivity Image Reconstruction in MREIT*, SIAM J. Appl. Math. **70**(2010), Issue 8, pp. 2883–2903.
[31] Q. Ma and B. He, *Investigation on magnetoacoustic signal generation with magnetic induction and application to electrical conductivity reconstruction*, Phys. Med. Biol., **52** (2007), pp. 5085–5099.
[32] J. Malý, D. Swanson, and W. P. Ziemer, *The co-area formula for Sobolev mappings*, Trans. Amer. Math. Soc. **355**(2003), no. 2, 477-492.
[33] N. Mandache, *Exponential instability in an inverse problem for the Schrdinger equation,* Inverse Problems **17** (2001), pp. 1435–1444.
[34] J. R. McLaughlin and J. -R. Yoon, *Unique identifiability of elastic parameters from time-dependent interior displacement measurement*, Inverse Problems**20**(2004), pp. 25-46.
[35] A. Nachman, A. Tamasan, and A. Timonov, *Conductivity imaging with a single measurement of boundary and interior data*, Inverse Problems, **23** (2007), pp. 2551–2563.
[36] A. Nachman, A. Tamasan, and A. Timonov, *Recovering the conductivity from a single measurement of interior data*, Inverse Problems, **25** (2009) 035014 (16pp).
[37] A. Nachman, A. Tamasan, and A. Timonov, *Reconstruction of Planar Conductivities in Subdomains from Incomplete Data*, SIAM J. Appl. Math. **70**(2010), Issue 8, pp. 3342–3362.
[38] M. Z. Nashed and A. Tamasan, *Structural stability in a minimization problem and applications to conductivity imaging*, Inverse Probl. Imaging, **4** (2010) to appear.
[39] S.H. Oh, B. I. Lee, E. J. Woo, S. Y. Lee, M. H. Cho, O. Kwon, and J. K. Seo, *Conductivity and current density image reconstruction using B_z algorithm in magnetic resonance electrical impedance tomography*, Phys. Med. Biol. **48**(2003), pp. 3101–3116.
[40] S. Onart, Y.Z. Ider, and W. Lionheart, *Uniqueness and reconstructions in magnetic resonance -electrical impedance tomography (MR-EIT)*, Physiol. Meas. **24**(2003), pp. 591–604.
[41] C. Park, O. Kwon, E.J. Woo, and J. K. Seo, *ELectrical conductivity imaging using gradient B_z decomposition algorithm in magnetic resonance electrical impedance tomography (MREIT)*, IEEE Trans. Med. Imag. **23**(2004), pp. 388–394.
[42] G. C. Scott, *NMR imaging of current density and magnetic fields*, Ph.D. dissertation, Univ. Toronto, Toronto, Canada, 1993.
[43] G. C. Scott, M. L. Joy, R. L. Armstrong, and R. M. Henkelman, *Measurement of nonuniform current density by magnetic resonance*, IEEE Trans. Med. Imag., **10** (1991), pp. 362–374
[44] P. Sternberg and W. P. Ziemer, *Generalized motion by curvature with a Dirichlet condition*, J. Differ. Eq., **114**(1994), pp. 580–600.
[45] P. Sternberg and W. P. Ziemer, *The Dirichlet problem for functions of least gradient. Degenerate diffusions* (Minneapolis, MN, 1991), 197–214, in IMA Vol. Math. Appl., 47, Springer, New York, 1993.
[46] E. J. Woo and J. K. Seo, *Magnetic resonance electrical impedance tomography (MREIT) for high resolution conductivity imaging*, Physiol. Meas., **29** (2008), pp. R1-R26.
[47] L. V. Wang, *Prospects of photoacoustic tomography*, Medical Physics**35**(2008), 5758-5767.
[48] N. Zhang, *Electrical impedance tomography based on current density imaging*, M.Sc. Thesis: University of Toronto, Canada, 1992.

Adrian Nachman, Department of Mathematics and Edward S Roger Sr. Department of Electrical and Computer Engineering, University of Toronto, Toronto, Ontario, Canada

E-mail address: nachman@math.toronto.edu

Alexandru Tamasan, Department of Mathematics, University of Central Florida, 4000 Central Florida Blvd., Orlando, FL, 32816, USA

E-mail address: tamasan@math.ucf.edu

Alexander Timonov, Division of Mathematics and Computer Science, University of South Carolina Upstate, 800 University Way, Spartanburg, SC 29303, USA

E-mail address: atimonov@uscupstate.edu